H-mode Threshold Power Dependences in ITPA Threshold Database

ITPA H-mode Threshold Database Working Group 1), presented by Y.R.Martin 2)

1) from Alcator C-Mod: J.A.Snipes, M.Greenwald;
ASDEX/ASDEX Upgrade: F.Ryter, O.J.W.F.Kardaun, J.Stober;
COMPASS-D/MAST: M.Valovic;
DIII-D: J.C.DeBoo;
JET/EFDA: Y.Andrew, J.G.Cordey, R.Sartori, K.Thomsen;
JFT-2M/JT-60U: T.Takizuka, Y.Miura, T.Fukuda, Y.Kamada, K.Shinohara, K.Tsuzuki;
PBX-M/NSTX: S.M.Kaye, C.Bush, R.Maingi;
TCV: Y.R.Martin;
TUMAN-3M: S.Lebedev.

2) CRPP, Association EURATOM-Confédération Suisse, EPFL, CH-1015 Lausanne, Switzerland

e-mail contact of main author: yves.martin@epfl.ch

Abstract.

Newly contributed data and the current status of the International H-mode threshold database are presented. Selecting data from only one divertor geometry per tokamak leads to a reduction in the data scattering and improves the quality of the fits. The selection of a reduced set of transition types also leads to fit improvement. A new parameter, (R+a)/(R-a), is introduced in the power law scaling to account for the data provided by the spherical tokamaks. A prediction for ITER is given for the different power law scalings. Threshold power for ITER is estimated at about 35MW.

1. Introduction

The ELMy H-mode is obtained in many tokamaks. Its good confinement properties together with its good impurity removal make it the nominal operational regime for ITER. It is widely accepted that the transition from L-mode to H-mode (LH transition) is obtained when the input power exceeds a threshold, which depends on the plasma density and the magnetic field [1,2]. The threshold power was generally found to be lower when the plasma is shaped in a single null diverted configuration with the ion gradB drift directed towards the X-point. Finally, it also depends on other parameters such as the plasma shape, the neutral density or the vacuum vessel conditioning, but in a less clear manner.

The comparison of the threshold power measured in different tokamaks under different conditions has shown a relationship between that power and the plasma size. Therefore, data from a series of tokamaks have been collected into one database to analyse the size dependence of the H-mode threshold power. After data selection, power law scalings were deduced, including the plasma density, magnetic field and parameters describing the plasma size. Finally, the power law scaling is used for extrapolation to new devices such as ITER. Practically, the international H-mode threshold database (IGDBTH), initiated in 1992 and summarised in [3], now contains data from 13 tokamaks: Alcator C-Mod, ASDEX, ASDEX Upgrade, Compass, DIII-D, JET, JFT-2M, JT-60U, MAST, NSTX, PBX-M, TCV and TUMAN-3M.

In the analyses, the experimental threshold power is approximated by the loss power P_L measured just before the transition. $P_L=P_{OHM} + P_{AUX}$ - dW/dt (PLTH in database) where P_{OHM} is the Ohmic power [MW], P_{AUX} the absorbed auxiliary heating power [MW] and dW/dt the time derivative of the total plasma energy [MJ/s]. At the last IAEA conference, two power law scalings were presented. They were based on data from 9 tokamaks (ASDEX, ASDEX Upgrade, Alcator C-Mod, COMPASS-D, DIII-D, JET, JFT-2M, JT-60U, TCV) and their expressions were [4]:

$$P_{th1} = 1.67\ n_{e20}^{0.61}\ B_T^{0.78}\ a^{0.89}\ R^{0.94} \qquad \text{RMSE=25.1\%} \qquad (1)$$

$$P_{th2} = 0.05\ n_{e20}^{0.46}\ B_T^{0.87}\ S^{0.84} \qquad \text{RMSE=26.0\%} \qquad (2)$$

where P_{th}, n_{e20}, B_T, a, R, and S are respectively the predicted threshold power [MW], plasma density [$10^{20}m^{-3}$], magnetic field [T], minor radius [m], major radius [m] and plasma outer flux surface area [m^2].

Since 2002, new data have been added to the database. This paper introduces the new data and summarises the present status of the database. It then shows the analysis of the database, the criteria used for data selection and to the parameter selection to reduce the Root Mean Square Error (RMSE) of the fit. The role of the effective charge (Z_{eff}) and the absolute B was studied in [5] and will not be discussed here. Finally, a new estimation of the prediction for ITER is given.

2. New Data

New time slices were provided by ASDEX Upgrade (17 new time slices), Alcator C-Mod (79), JET (555), MAST (6), NSTX (6) and TCV (13). The ASDEX Upgrade new contribution consists of transitions obtained at low density. For Alcator C-Mod, LH transitions in inner wall limited, inner nose limited, single null and double null configurations, as well as low density time slices were provided. New JET data points come from 2002 and 2003 campaigns with the MKII GB (SRP) divertor as well as 2001 discharges performed in H or He. The MAST contribution comes from new double null discharges. A first set of data points was provided by NSTX. Data taken at LH transitions obtained in ohmic power ramps were provided by TCV as well as one LH transition obtained with ECH. The database now contains 7673 time slices.

At the beginning of the study presented in this paper, the data selection includes the largest possible data set. The phases taken into account are LD (D for dithering), DH and LH transitions, D for data points during the dithering phase and LDL, LHL for brief attempts to reach the H-mode. Data selection is restricted to time slices taken from plasmas in "appropriate conditions", as defined by a series of flags (SELDB). "Appropriate conditions" refers to single null configuration with ion gradB drift directed towards the X-point, a D_2 plasma with low radiated power. To avoid an increased threshold, the safety factor must be above 2.5, the density above a value defined in each tokamak and the plasma wall distance large enough. Exceptions to this rule were allowed to either extend the study to such parameters or avoid elimination of a complete data set provided by a particular device. For instance, the Single Null condition would reject all Tuman-3M data. Therefore, an exception was made for the corresponding data points to maintain them in the preliminary analysis.

Table 1 shows a comparison of the contribution from the different tokamaks in the selected datasets. The improvement from 665 to 1339 time slices comes from the new data contributions, as listed at the beginning of the section, and from the extension of the dataset.

The exceptions to the "appropriate conditions" are: 2 entries in Hydrogen plasmas and 29 in Helium for JET; 24 data points in Double Null configuration for JET, 15 for MAST and 5 for PBX-M; 15 time slices in Limited configuration for TUMAN-3M; 46 entries with unfavourable ion gradB drift for Alcator C-Mod.

A second data set was defined under the name IAEA04R. It contains all data in "appropriate conditions" and only those exceptions which keep the diversity of the database. As an example, MAST and PBX-M Double Null data are kept but JET Double Null data are rejected. JET non D_2 data are also rejected. This restricted data set contains 1298 entries.

TABLE 1: Contributions from tokamaks to the full dataset on LH transitions

Tokamak	**IAEA02**	**IAEA04**
ASDEX	37	43
ASDEX Upgrade	172	232
Alcator C-Mod	130	230
COMPASS-D	8	18
DIII-D	55	58
JET	118	610
JFT-2M	41	53
JT-60U	58	58
MAST		20
NSTX		6
PBX-M	5	5
TCV	41	51
TUMAN-3M		15
Total	**665**	**1399**

3. DataBase Status

The database completed with all new data is referred to as IGDBTH4v4. It contains 7673 entries. Among those, 1399 time slices belong to the large dataset as described above. The remaining time slices either belong to other phases of a discharge (L-mode, H-mode or HL transition) or have at least one parameter which is outside the "appropriate conditions". The restricted dataset contains 1298 time slices. All are in D2 working gas. All are in Single Null configuration but those from MAST (15 DN), PBX-M (5 DN) and TUMAN-3M (15

TABLE 2: Number of data points for all PHASE and TOKAMAK

	PHASE								
Count	D	DH	LD	LDL	LH	LHL	OHMD	OHMH	
ASDEX	0	0	0	0	37	6	0	0	43
AUG	18	6	89	22	82	0	10	5	232
CMOD	46	0	24	0	49	3	27	35	184
COMPASS	10	0	1	0	0	0	6	1	18
D3D	1	2	0	0	53	0	0	2	58
JET	226	66	91	0	172	0	0	0	555
JFT2M	12	0	6	0	35	0	0	0	53
JT60U	0	0	36	0	22	0	0	0	58
MAST	0	0	0	0	4	0	16	0	20
NSTX	1	0	0	0	5	0	0	0	6
PBXM	0	0	0	0	5	0	0	0	5
TCV	0	20	0	0	1	0	16	14	51
TUMAN-3M	0	0	0	0	0	0	0	15	15
	314	94	247	22	465	9	75	72	1298

LIM). All are in favourable ion Grad B drift but those in Double Null configuration.

The parameter PHASE describes more precisely in which part of the L-mode to H-mode transition the time slice was taken. OHM, L, D, H refer to Ohmic, L-mode, Dithering and H-mode, respectively, all combinations of these references indicate transitions from one to the next state. Usually data corresponding to a transition are taken just before its occurrence. A 'D' alone represents a time slice taken during the dithering phase. Table 2 shows the contribution of all tokamaks through the different PHASEs.

As shown in Table 2, the restricted data set contains 712 entries at LD or LH transitions (55%). 147 time slices (11%) also correspond to the transition out of the L-mode but are obtained in ohmic condition. 408 data points (32%) are taken during the dithering phase which is considered as being at the threshold as well. The remaining 31 entries (2%) are also considered as at the threshold since they show an attempt to go in H-mode even if they return to L-mode soon after.

Figure 1a and 1b show the distribution of the plasma density and magnetic field, respectively, for each device. The high magnetic field capability of Alcator C-Mod is clearly visible in both magnetic field and plasma density distributions. The magnetic field is quite uniform for half the tokamaks.

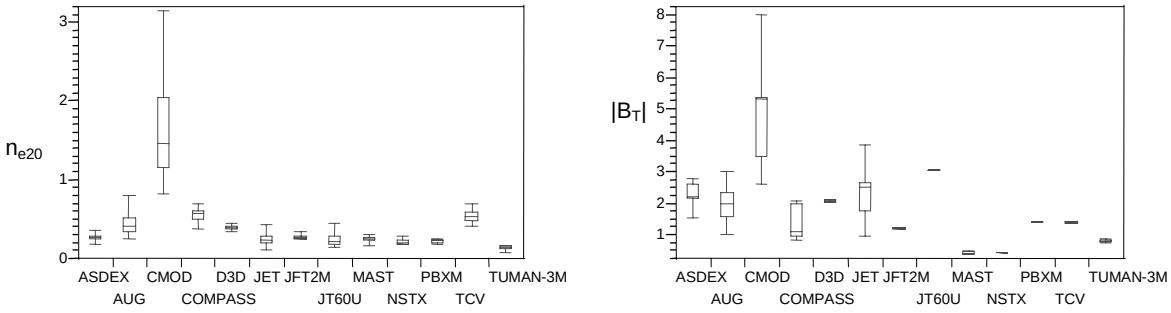

Figure 1: Distribution of plasma density and magnetic field for each tokamak. Quantile box plots indicate the minimum, 25%, 50 %, 75% and maximum of the distribution.

4. Analysis

4.1 General fit

The fits for the threshold power were generally based on two sets of variables: [n_{e20}, B_T, a, R] and [n_{e20}, B_T, S]. In this paper the first one will be used as a reference. With the restricted data set (1298 data points because of missing data), the fit gives:

$$P_{th3} = 3.46\ n_{e20}^{0.48}\ B_T^{0.65}\ a^{1.37}\ R^{0.26} \qquad \text{RMSE=32.4\%} \qquad (3)$$

The a and R dependences are significantly different from fit (1). However, since most tokamaks have the same aspect ratio, the roles of a and R are quite exchangeable and then the size dependence is comparable. This correlation of a and R can only be removed with a larger contribution from the Spherical Tokamaks. Nevertheless, it is their presence in the fit which already induces the change in the expression. The influence of Spherical Tokamaks on the fit will be addressed later.

The deviation of the actual threshold power (P_L) from the fit is shown in Fig.2. Data from TUMAN-3M remain out of the fit and the excess in the threshold is due to the fact that all data points are taken while in limited configuration. NSTX also show an excessive threshold power with this set of variables. Data points from spherical tokamaks (NSTX and

MAST) and TUMAN-3M are therefore removed from the data set to analyse the effect of the divertor type among conventional tokamaks operating in diverted configuration.

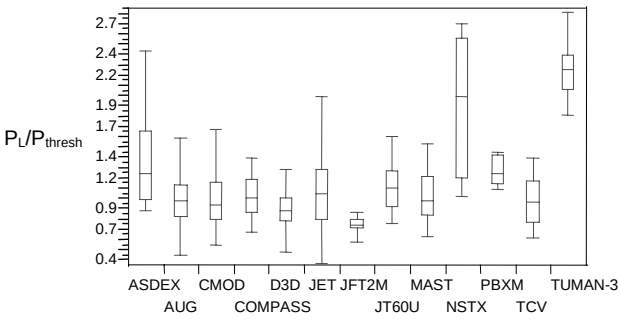

Figure 2: Deviation of the threshold power from the fit for each tokamak

4.2 Effect of divertor

The database contains a variable indicating the name of the divertor which was used for the experiments (DIVNAME). The effect of the divertor shape can then be treated and used for data selection. Figure 3 shows the deviation of the threshold power as a function of the divertor name for JET data.

LH transitions in plasmas with Mk0, MkI or MkIIap divertors have an average threshold power below the value given by the fit (1). Since the database contains a larger variety of data points with the MkIIap divertor, these time slices will be used in further analysis.

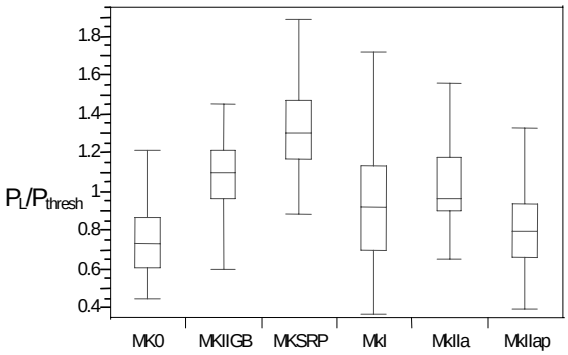

Figure 3: Deviation of the threshold power from the fit for each divertor in JET

The same analysis is done for ASDEX and ASDEX Upgrade and DIV-I gives a smaller threshold. The closed divertor is chosen for Alcator C-Mod and JT-60U, as expected from the fact that closed divertors are more suited to keep the plasma impurity level low. Since closed divertors are chosen and TCV works with an open divertor, TCV is removed from the data set. Table 3 summarises the selected divertor for the tokamaks which changed divertor configuration.

TABLE 3: Selected divertors

Tokamak	Divertor
ASDEX	DIV-I
ASDEX Upgrade	DIV-I
Alcator C-Mod	DIVCLOSE
JET	MkIIap
JT-60U	CLOSEDSN

With this restriction to one divertor per tokamak, the number of data points decreases to 462 and the new fit is:

$$P_{th4} = 2.96\, n_{e20}^{0.85}\, B_T^{0.51}\, a^{1.07}\, R^{0.83} \qquad \text{RMSE=22.9\%} \qquad (4)$$

The RMSE is much smaller with this restricted dataset indicating that the type of divertor plays an important role in the data scattering. Compared to the global fit (3), the dependence in plasma density is, here, stronger and in the magnetic field weaker, while the dependence in plasma size remains similar. In comparison, the fit calculated with the JET

MKII GB (SRP) divertor, which induces a higher threshold power in JET, gives a stronger dependence in a and R, 1.55 and 0.53 respectively. Figure 4 shows the reduction of the scattering in the comparison between experimental and estimated threshold power when only one divertor is selected.

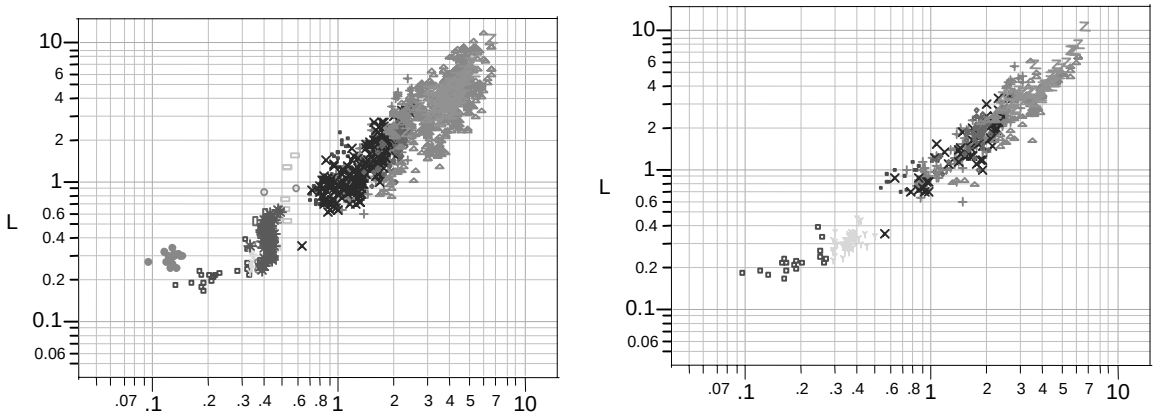

$3.46\ n_{e20}^{0.48}\ B_T^{0.65}\ a^{1.37}\ R^{0.26}$ $2.96\ n_{e20}^{0.85}\ B_T^{0.51}\ a^{1.07}\ R^{0.83}$

Figure 4: Comparison between the experimental and estimated threshold power for the fits (3) and (4), corresponding to the global dataset and the restricted to one divertor per tokamak dataset.

4.3 Influence of the phase in the transition process

In the previous fit, the selected data have the PHASE variable equals to either D, DH, LD, LDL, LH, OHMD or OHMH. In this subset, ASDEX Upgrade data contain all LDL time slices (22). These time slices show an experimental threshold power much bigger than the estimated power as well as the average power, as shown in Fig.5. This is in contradiction with the fact that these data points could be just at the threshold. Nevertheless, these time slices are removed from the dataset. Similarly, OHMH data are removed for ASDEX Upgrade.

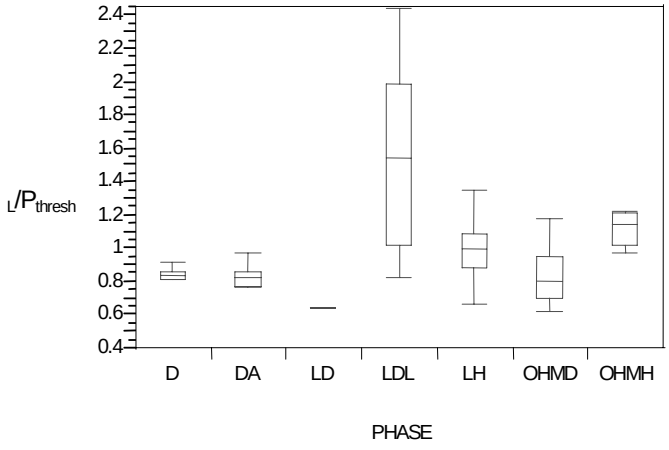

Figure 5: Deviation of the threshold power from the fit for each PHASE in ASDEX Upgrade

The same filtering is applied to all other tokamaks and TCV rejoins the dataset since its data is well aligned with the scaling. This data set contains 461 time slices and the fit is:

$$P_{th5} = 2.34\ n_{e20}^{0.67}\ B_T^{0.62}\ a^{1.02}\ R^{0.71} \qquad \text{RMSE=21.5\%} \qquad (5)$$

The RMSE is lower than in the previous fit. The exponents for a and R are slightly reduced.

In this dataset, each tokamak contributes with a quite different weight: JET has 113 data points while PBX-M has only 5. A random selection is performed to reduce the large datasets (JET and ASDEX Upgrade) to approximately 50 samples to match the population of most of the remaining ones (Alcator C-Mod, DIII-D, JFT-2M, JT-60U and TCV). The dataset is then reduced to 367 entries. The RMSE value is slightly reduced but the coefficients of the fit remain quite similar, independently of which data is kept for ASDEX Upgrade and JET.

4.4 Effect of the parameter set

The new fits presented in this paper so far are based on the plasma density, magnetic field, plasma minor and major radius. Fits are also calculated with the plasma outer surface area instead of a and R. The results are very similar. The effect of the aspect ratio $\varepsilon = a/R$ cannot be determined with this parameter set. Similarly, the plasma shape can play a non-negligible role in the threshold power as seen in TCV [6]. Therefore, an extension of the parameter set could lead to a more precise fit of the threshold power. However, it is necessary to select parameters which are not a combinations of the others, such as the aspect ratio taken with a and R in the fit. Typically the shape and size of a plasma can be defined by 3 independent parameters, for instance: a or R, κ (plasma elongation) or S, ε or $R_{mm}=R_{max}/R_{min}=(R+a)/(R-a)$. The latter parameter also describes the aspect ratio, although differently. Fits using different combinations of these parameters are calculated with the dataset used for (5) enlarged with MAST and NSTX data, since these devices widen significantly the range in aspect ratio or R_{mm}. 412 time slices make up this dataset. The fit using only a and R is compared to the best fit of this family, that found with R, S and R_{mm}:

$$P_{th6} = 3.73\ n_{e20}^{0.55}\ B_T^{0.60}\ a^{1.43}\ R^{0.18} \qquad \text{RMSE=24.5\%} \qquad (6)$$

$$P_{th7} = 0.151\ n_{e20}^{0.63}\ B_T^{0.67}\ R^{1.22}\ S^{0.25}\ R_{mm}^{1.21} \qquad \text{RMSE=22.9\%} \qquad (7)$$

The parameter R_{mm} leads to an RMS error smaller than that obtained with the aspect ratio. Since this parameter is proportional to the ratio of the toroidal magnetic field taken at the high field and low field side of the plasma edge ($B_{T(in)}/B_{T(out)}$), it indicates the importance of the strength of the magnetic field at the plasma edge as already shown in [5].

The LH transition threshold power was found to depend on the X-point height above the divertor floor [7,8]. Including this variable in the parameter set leads to a reduction in the RMS error of the fit, down to 18%. However, this reduction is partly due to a substantial reduction of the dataset since only 203 time slices are used in this calculation. An improvement of the database would therefore be required to address this question.

4.5 Prediction for ITER

Power law scalings presented in this paper are used to estimate the LH threshold power for ITER (R=6.2m; a=2m; $S=678m^2$; $n_{e20}=0.610^{20}m^{-3}$; B=5.3T) as shown in Table 4. The uncertainty is calculated as the standard error in prediction.

The low value of the prediction with scaling P_{th3} (3) is due to the participation of small devices with a high threshold power in the fit, which induces a tilt in the fit and therefore an under estimation when extrapolating to large devices. In case of scaling P_{th6} (6), the prediction is biased by the presence of the spherical tokamaks in the traditional fit with plasma density, magnetic field, major and minor radii. With the set of parameter used for this scaling, they also induce a similar tilt than in scaling P_{th3}.

TABLE 4: Threshold power for H-mode access in ITER

Scaling	Threshold power [MW]
P_{th1}	46
P_{th2}	40
P_{th3}	32 - 35
P_{th4}	40 - 45
P_{th5}	32 - 37
P_{th6}	27 - 31
P_{th7}	32 - 37

Scalings P_{th5} (5) and P_{th7} (7) are based on a large set of devices and data points. They have a modest RMSE and their residuals are independent of the plasma size. These scalings can therefore be taken as the reference for estimating the threshold power in future devices. Both give the same predicted threshold power for ITER.

5. Conclusions

New data have been added into the International H-mode threshold database which now contains 7673 time slices from 13 tokamaks. The initial dataset is enlarged (1298 time slices), including new data and data taken during the dithering phase.

After selecting data from the best divertor for each device and from the best LH transition times, according to the DIVNAME and PHASE parameter respectively, the RMSE of the fit was lowered down to 22.9%. In this fit most devices are represented, improving the data range and therefore the reliability of the fit.

With the addition of a new parameter in the fit, (R+a)/(R-a), and the use of the major radius and the plasma surface for the plasma geometry description, the Spherical Tokamaks, MAST and NSTX, are well fitted.

The predicted threshold power for ITER reaches 35MW when the best fits are used.

Acknowledgement

This paper could not have been written without the contribution of the teams working on tokamaks providing data to the International H-mode Threshold Database. The authors would like to thank them all.

References

[1] ASDEX Team, Nucl. Fus. 29 (1989) 1959
[2] Burrell K H et al. Plasma Phys. and Contr. Fusion 31 (1989) 1649
[3] Ryter F et al. Nucl. Fus. 36 (1996) 1217
[4] Snipes J A et al. 19th IAEA Fus. Energy Conf. IAEA-CN-94/CT/P-04
[5] Takizuka T et al. Plasma Phys. and Contr. Fusion 46 (2004) A227
[6] Martin Y R et al. Plasma Phys. and Contr. Fusion 44 (2002) A143
[7] Carlstrom T N et al. Proc. of 16th European Conference on Controlled Fusion and Plasma Physics, Vol 13B (1989) 241
[8] Andrew Y et al. Plasma Phys. and Contr. Fusion 46 (2004) A87